Multi-phase Wireless Power Transfer with High Power Density Inductive Coils for Electric Drone Charging

Lucas A. Gastineau
SPARK Lab, Pigman Eng. College
University of Kentucky
Lexington, KY, USA
lucas.gastineau@uky.edu

Donovin D. Lewis
SPARK Lab, Pigman Eng. College
University of Kentucky
Lexington, KY, USA
donovin.lewis@uky.edu

Omer Onar
Vehicle Power Electronics Group
Oak Ridge National Laboratory
Knoxville, TN, USA
onaroc@ornl.gov

Dan M. Ionel
SPARK Lab, Pigman Eng. College
University of Kentucky
Lexington, KY, USA
dan.ionel@ieee.org

***Abstract*—Wireless charging of unmanned ground vehicles and aircraft has been proposed to increase charging reliability and security, allow for autonomous functionality, and either reduce battery size or increase continuous flight time. This paper proposes a three-phase Litz wire primary and a two-phase PCB secondary for high secondary-side power density considering misalignment tolerances, surface and volumetric power density, and coil sizing. Electromagnetic 3D finite element analysis (FEA) simulations are conducted to study variation in mutual inductance and coupling coefficient with different secondary coil sizes and number of turns, horizontal and vertical misalignment between the primary and secondary, and a combination of both for a set of designs with the same rated power. Results indicate that receiver coils of reduced size relative to the primary can deliver rated power for increased power density and higher tolerance to misalignment.**

***Index Terms*—Wireless power transfer, inductive coupler, multi-phase systems, wireless charging, unmanned aerial vehicles**

I. Introduction

Inductive wireless power transfer (WPT) systems use high-frequency excitation to generate electromagnetic fields coupling and transferring power between two coils. Implementation of wireless charging systems may improve reliability and autonomy in battery-powered electronics, including robotics, unmanned aircraft vehicles (UAV), and small appliances [1]. Enhanced battery capacity factor through the application of WPT may reduce necessary battery size, consequently reducing volume, weight, and dependence on critical materials.

Wireless charging capabilities for UAVs, as depicted in Fig. 1, can enable autonomous functionality, reduce the necessary battery size for the intended flight profile, and minimize human interaction for operation [2]. Previous studies of WPT design for UAV systems are typically designed to operate in ranges from 300W to 750W [3]–[5] and have focused on improving gravimetric power density [6], [7] and misalignment tolerance between coupled coils [8], [9]. Methods to increase power density are a topic of interest in wireless charging design, requiring innovations in coil geometry or systematic design to mitigate reductions in efficiency typical of reduced coil outer diameter (OD) [10], [11].

Multi-phase coil configurations, such as the one seen in Fig. 1, have been proposed to increase power density, field utilization, and reduce voltage stress and receiver-side current ripple compared to conventional single phase coils [12]. The studied phase-per-layer bipolar double-D type coils are capable of a number of phase combinations, which can enhance the transferred power for the same surface area as previously studied in [13]. Within that study, the two-phase coil configuration was found to have advantages including electromagnetic isolation between phases on the same side, and naturally balanced inductances and induced voltages, which can significantly reduce overall volume and complexity on the secondary side. The proposed combination of three-phase on the transmitting coil and two-phase on the secondary coils was found to increase the output power by a factor of three relative to a single-phase coil at the same OD.

This paper proposes a high-power density polyphase coil for wireless charging of UAVs and a process for integrated machine learning design. Finite element analysis (FEA) was used to simulate the electromagnetic performance of two, three, and three-to-two phase macro-coil models for mutual inductances and coupling coefficients with varying dimensions and conditions. Consideration is given to stranded Litz wire, PCB-type trace coils, and topologies consisting of a combina-

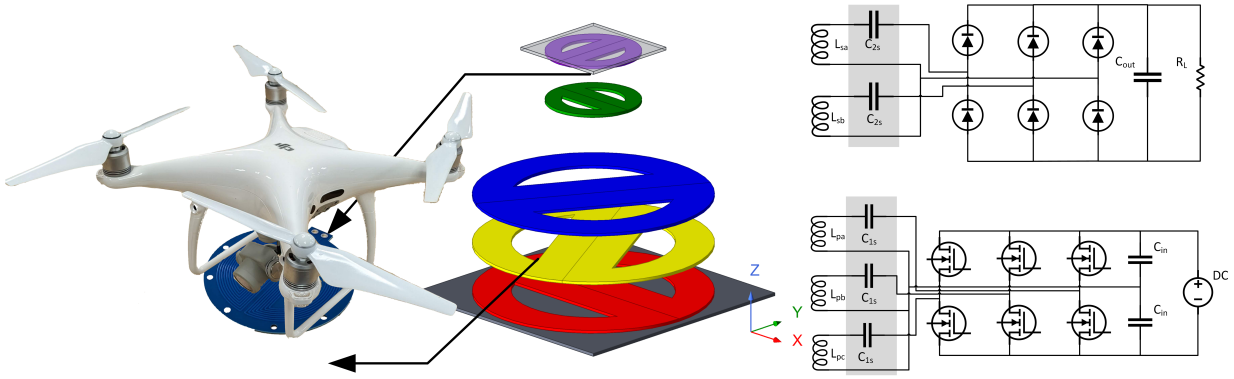

Fig. 1. Example inductive PCB-type coil setup for stationary wireless charging of an electric drone. The charging coil can be positioned at the base or wrapped around the legs of the drone landing gear. Exploded view of the substantially different coupling coils on the primary and secondary side with a schematic of the power electronics. The two-phase coils are electrically and mechanically shifted by 90 degrees and three-phase coils by 120 degrees.

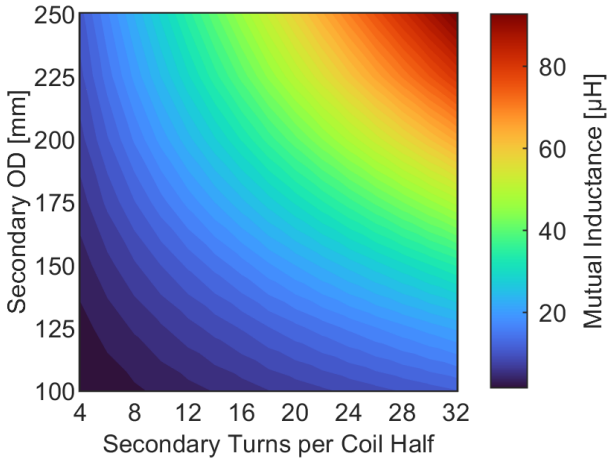

Fig. 2. Resulting mutual inductance from a parametric study of receiver coil OD and turns. Models with the same mutual inductance are ideally capable of the same power output but can have varying misalignment tolerance.

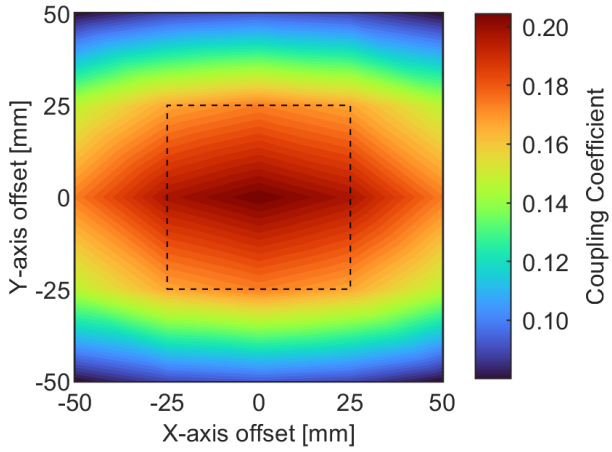

Fig. 3. Misalignment tolerances of a three-to-two phase model with 250mm primary OD and 100mm secondary OD. Misalignments will affect models differently based on coil configuration and connections type.

tion of both coil types.

II. UAV and Wireless Charging Specifics

Typical objectives for WPT systems for drones are minimal volume and weight on the secondary-side and maximum misalignment tolerance at rated power. As a majority of the constraints are on the receiver side, the volume on the primary side was assumed to be unrestricted. With these assumptions in mind, different sizing of coil OD allows for large transmitting coils, which are typically not application constrained, and small receiver coils to minimize the impact of integration on flight characteristics. A larger coil OD increases the mutual inductance, which can either allow for fewer turns or a reduction of current and associated copper losses.

Design of inductive coils for UAVs considering the constraints of volume and weight requires detailed studies of transferred power and misalignment tolerance. The output power in a multi-phase system can be calculated using the following equation:

$$P = j\omega I_s^H \underline{M}_{ps} I_p \approx K_p \omega M_{ps} I_s I_p, \tag{1}$$

where K_p represents the multi-phase model specific scaling coefficient, $\underline{M}_{ps}$ is the maximum mutual inductance term between a single phase of the primary and secondary, I_s is the secondary current, and I_p is the primary current [12]. Under perfect alignment, in a three-to-two phase system the output phase current can be calculated as:

$$I_j = \frac{\sum j\omega M I}{Z_j}, \tag{2}$$

where Z is the phase impedance [14]. The output current of a multiphase system must be considered when sizing coils and considering phase configurations.

The use of a three-to-two phase topology combined with PCB-type coils is uniquely suited for WPT applications with drones, as it benefits from a K_p of 3, increasing power relative to a single phase coil while reducing the number of conductors and volume on the secondary side. Simulated mutual inductances between phases are given as:

$$\begin{bmatrix} M_{SAPA} & M_{SAPB} & M_{SAPC} \\ M_{SBPA} & M_{SBPB} & M_{SBPC} \end{bmatrix} = \begin{bmatrix} 43.4 & -20.9 & -20.9 \\ 0.1 & 37.1 & -37.1 \end{bmatrix} \mu H, \tag{3}$$

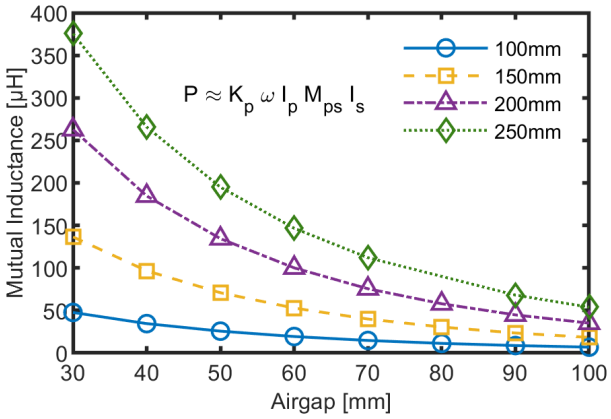

Fig. 4. Simulated mutual inductance between the primary and secondary side phase A coils with varying secondary OD and airgap length.

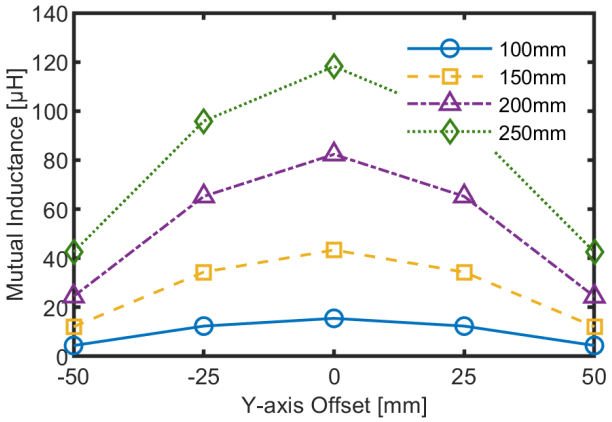

Fig. 5. Mutual inductance between the primary and secondary for secondary ODs at 16 turns per coil half. Deviations in mutual inductance with offsets grow smaller as the coils become largely different.

where subscripts P and S indicate primary and secondary side coils, and A, B, and C designate the phase. A two-phase receiver configuration has electromagnetically isolated phases on the secondary, which may increase voltage excitations compared to alternative phase configurations.

Wireless drone charging misalignment tolerance needs to be maximized due to the high number of degrees of freedom and overall impact on system performance. Horizontal coil-to-coil misalignments can result in large variations in mutual inductances and induced voltages, which can substantially affect system performance depending on the coil geometry and resonant tuning network [15], [16]. Vertical misalignments also significantly determine effective coupling between coils and requires a transmitting coil outer diameter multiple times larger than the size of the airgap. Coupling coefficient, $k = \frac{M}{\sqrt{L_1 L_2}}$, is a metric which characterizes the effective coupling between the primary and secondary coils and can be used to compare between varied cases of coil misalignment.

III. Inductive Coil Design Studies

A three-to-two phase macro coil model was developed in ANSYS Maxwell [17], to simulate the electromagnetic characteristics of various coil sizes and relative misalignments between the primary and secondary within an example case study. The macro coil represents a bundle of insulated conductor strands, which are used to mitigate AC losses at high-frequency and can be physically constructed with Litz wire or PCBs. The model employed in this study was previously validated experimentally by comparing simulated inductances with LCR meter measurements of a 100mm OD prototype PCB coil with satisfactory agreement of less than 10% error.

The parameterized simulation coils were designed to operate at 85kHz with a primary coil size of 250mm OD, square ferrite core on the outside face of the primary and secondary coils of 265mm width and 3mm thickness, and varying secondary coil size. Coil width was maintained at 67% of the usable space in each coil half resulting from previous studies maximizing coupling coefficient. An airgap of 80mm was selected for the case study as it results in a 0.2 coupling coefficient with a secondary coil sized for 250mm OD, selected to maximize OD to airgap ratio while allowing for decent efficiency. Four designs were constructed at varying ODs employing selected number of turns to reach the same primary to secondary mutual inductance following a parametric study of turns and OD with results as depicted in Fig. 2.

The designs at 100mm, 150mm, 200mm, and 250mm outer diameters were simulated at varying vertical and horizontal misalignment to evaluate their respective change in mutual inductance. An example worst-case scenario of horizontal misalignment is shown in Fig. 3 using the secondary coil design with the smallest outer diameter. It should be noted that there is a region of relative coupling coefficient homogeneity, as indicated with the dashed box on Fig. 3, which is dependent on primary and secondary coil OD. With this in mind, alternative methods to systematic coil design for misalignment include automatic transmitter reposition such as reported prior in [18].

IV. Results and Discussion

Results from the example case study include simulated mutual inductance and coupling coefficient with parametric studies of outer diameter, turns, and receiver misalignment. Simulated mutual inductance as a result of varying secondary coil OD and turns are depicted in Fig. 2 at a 40mm airgap. The results revealed that there are bands within which the same mutual inductance can be reached for different combinations of OD and turns. For example, to reach a mutual inductance of 30µH, the 100m, 150mm, 200mm, and 250mm ODs coils would require 8, 12, 24, and 64 turns per coil, respectively. Ideal surface area-related power densities for the 4 coil designs are 12, 9, 3, and $2kW/m^2$ respectively at 700W.

The offsets in alignment of coils have significant effects on coupling between coils, similar to the variation in coupling coefficient depicted for the worst-case example in Fig. 3. Coupling coefficient and mutual inductance variation were recorded for each study but resulted in very similar patterns of variation. Results for increased airgap length or vertical spacing between the primary and secondary coil in Fig. 4 highlights

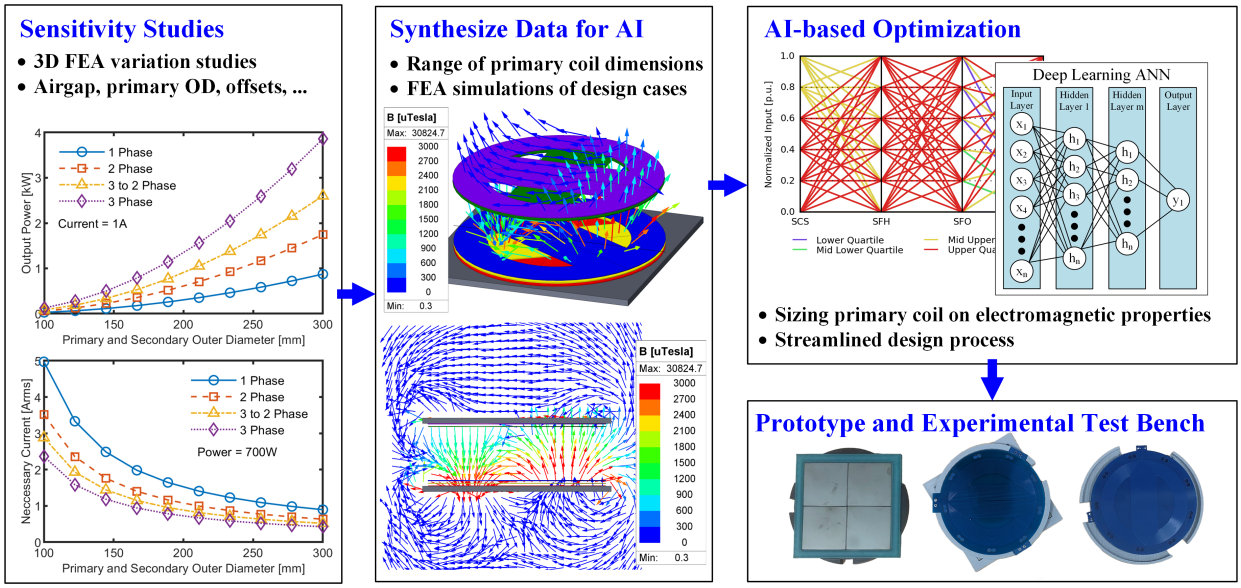

Fig. 6. Flow chart illustrating the proposed coil optimization process through FEA simulations and machine learning. Coil dimension sensitivity studies were completed to determine variation in mutual inductance, coupling coefficients, and induced voltages to determine appropriate sizing ranges. Electromagnetic FEA simulations proposed calculate magnetic characteristics of design candidates, which have been used to train a surrogate machine learning model for a fixed OD with potential extension to multiple ODs.

the importance of coil outer diameter in effective coupling across the airgap. As secondary-side coil OD increases, mutual inductance increases for the same airgap or the same mutual inductance can be achieved at a larger airgap.

Reduced size of the receiver coil OD relative to the transmitter can also reduce deviations in mutual inductance caused by horizontal misalignment. The difference in OD of the transmitting and receiving coil results in smaller variations in the coupling with offsets, as shown in Fig. 5. As the receiving coil becomes smaller than the transmitting coil, results indicate that the coupling may become increasingly tolerant to horizontal and vertical misalignment.

The electromagnetic properties simulated within the varying studies emulate what we would expect with Litz wire or PCB-type coils, which are employed minimize AC losses at high frequency. Copper fill factor, volume, cost, and manufacturing constraints, differ greatly between Litz wire and PCB-type coils [19]. PCB coils have significantly smaller volume and the potential for high configurability and low cost, however, have significantly smaller maximum copper fill factor with current manufacturing process limitations [20]. The comparatively unconstrained size of the transmitter coil enables the utilization of Litz wire, which otherwise may not be possible at small sizes due to wire bend radii restrictions.

System performance is dependent on both coupling between coils, system configuration including compensation tuning, and losses within the coils themselves. Estimation of AC resistance can be directly simulated for Litz wire in macro coil 3D models for various FEA solvers, however, methods for the estimation of losses in PCB coils are still underdevelopment, especially in geometries that are not axisymmetric. Prior studies, such as [21], have shown the capability for performance near Litz wire with systematic coil design, suggesting that PCB coils may be an ideal form factor in applications requiring minimal volume and weight. Combining both coil types with the largely different sizing can allow for high fill factor with low-loss Litz wire on the primary side and low-volume, high power density PCB-type coils on the secondary side.

Back-of-the-envelope estimations of volumetric power density can be estimated with approximate estimates of coil thickness but vary significantly depending on Litz wire insulation and bend radius. In an example 150mm OD 12 turn case for a 700W rated system, the rated current would be 4 Arms and the smallest wire gauge would be 16 AWG. Assuming the insulation-to-conductor ratio follows commercially viable Remington Industries [22] 14 AWG Litz wire, 16 AWG Litz wire would have a total diameter of 1.8mm thickness, resulting in a 12% difference per phase when compared with a typical PCB thickness of 1.6mm. If the bend radius of the Litz wire is not sufficient for the number of turns, then a smaller wire gauge with more turns or a larger wire gauge can be used with higher current, resulting in 1.4mm or 2.3mm or 12% to 40% difference in total volume. In heavily constrained geometries, Litz wire coils may have a lower volumetric power density or not be feasible for small designs with a high number of turns.

V. Machine Learning-Based Design Process

Conventional design of electromagnetic coils requires extensive simulation and testing when considering the sizing parameters, parallel paths, coil configurations, and design constraints specific to each application. Deep learning algorithms have previously been proposed to optimize coil modeling by predicting coil inductances with high accuracy [23], [24]. Machine learning may be employed to drastically reduce the time to optimize for minimal losses and volume at rated power

considering multiple factors, including the coil OD, number of turns, excitation currents, and airgap.

Through the proposed machine learning design process in Fig. 6, sensitivity studies will be conducted to select key nonlinear design parameters that can be optimized in a deep learning-integrated algorithm. A deep learning neural network can be trained using physics-based equations and a large dataset of 3D FEA electromagnetic design candidates to accurately predict the mutual inductance and coupling coefficient of a three-to-two phase system. The predicted mutual inductance and coupling coefficient results can then be used to analytically solve most characteristics of a design, including the induced voltage, power transfer, and self inductance.

VI. Conclusion

This paper investigates the electromagnetic performance of a polyphase three-to-two phase wireless power transfer system for application with UAVs. Design considerations for applications with electric drones vs electric vehicles are explored and the scalability of coil ODs with multiple airgap lengths are studied. Sensitivity studies are conducted to analyze mutual inductance and coupling coefficients of coils with varying dimensions and configuration. Misalignment tolerances of coils in different topologies are studied as offsets in coils can have substantial effects on implementations for drones.

A unique configuration is proposed with Litz wire coils for the primary coil due to the high fill factor and low losses, and a PCB-type coil on the secondary side for reduced volume and increased power density. Results indicate that a smaller secondary-side OD can deliver the same rated power, increase volumetric power density, and may improve tolerance to misalignment assuming sufficient mitigation of AC losses.

Acknowledgment

This work was supported by the National Science Foundation (NSF) Graduate Research Fellowship under Grant No. 2239063. The support of ANSYS Inc. and the University of Kentucky, the L. Stanley Pigman Chair in Power endowment is also gratefully acknowledged. Any opinions, findings, and conclusions or recommendations expressed in this material are those of the author(s) and do not necessarily reflect the views of the sponsoring organizations.

References

[1] H. Feng, R. Tavakoli, O. C. Onar, and Z. Pantic, "Advances in high-power wireless charging systems: Overview and design considerations," *IEEE Transactions on Transportation Electrification*, vol. 6, no. 3, pp. 886–919, 2020.

[2] P. K. Chittoor, B. Chokkalingam, and L. Mihet-Popa, "A review on uav wireless charging: Fundamentals, applications, charging techniques and standards," *IEEE Access*, vol. 9, pp. 69 235–69 266, 2021.

[3] Y. Zhao, S. Shen, F. Yin, and L. Wang, "A high misalignment-tolerant hybrid coupler for unmanned aerial vehicle wpt charging systems," *IEEE Transactions on Transportation Electrification*, vol. 11, no. 1, pp. 1570–1581, 2025.

[4] C. Cai, S. Wu, L. Jiang, Z. Zhang, and S. Yang, "A 500-w wireless charging system with lightweight pick-up for unmanned aerial vehicles," *IEEE Transactions on Power Electronics*, vol. 35, no. 8, pp. 7721–7724, 2020.

[5] S. Obayashi, Y. Kanekiyo, K. Sugaki, A. Watabe, H. Nakakoji, H. Ichikawa, and N. Takao, "750-w 85-khz inductive rapid charging system for mid-sized uav," in *2022 Wireless Power Week (WPW)*, 2022, pp. 605–609.

[6] M. Abdelraziq, S. Paul, F. Bartels, and Z. Pantic, "Optimization of efficiency and receiver-coil mass in an autonomous 700-W S-S IPT system for UAV applications," in *2023 IEEE Applied Power Electronics Conference and Exposition (APEC)*, 2023, pp. 803–810.

[7] A. Basu and D. Costinett, "Design and optimization of a 600 w wireless drone charger for high gravimetric power density," in *2025 IEEE Applied Power Electronics Conference and Exposition (APEC)*, 2025, pp. 3253–3260.

[8] C. Rong, X. He, Y. Wu, Y. Qi, R. Wang, Y. Sun, and M. Liu, "Optimization design of resonance coils with high misalignment tolerance for drone wireless charging based on genetic algorithm," *IEEE Transactions on Industry Applications*, vol. 58, no. 1, pp. 1242–1253, 2022.

[9] S. Wu, C. Cai, X. Liu, W. Chai, and S. Yang, "Compact and free-positioning omnidirectional wireless power transfer system for unmanned aerial vehicle charging applications," *IEEE Transactions on Power Electronics*, vol. 37, no. 8, pp. 8790–8794, 2022.

[10] R. Bosshard, J. W. Kolar, J. Mühlethaler, I. Stevanović, B. Wunsch, and F. Canales, "Modeling and η - α -Pareto optimization of inductive power transfer coils for electric vehicles," *IEEE Journal of Emerging and Selected Topics in Power Electronics*, vol. 3, no. 1, pp. 50–64, 2015.

[11] W. Shi, J. Dong, T. B. Soeiro, C. Riekerk, F. Grazian, G. Yu, and P. Bauer, "Design of a highly efficient 20-kw inductive power transfer system with improved misalignment performance," *IEEE Transactions on Transportation Electrification*, vol. 8, no. 2, pp. 2384–2399, 2022.

[12] J. Pries, V. P. N. Galigekere, O. C. Onar, and G.-J. Su, "A 50-kW three-phase wireless power transfer system using bipolar windings and series resonant networks for rotating magnetic fields," *IEEE Transactions on Power Electronics*, vol. 35, no. 5, pp. 4500–4517, 2020.

[13] D. D. Lewis, L. Gastineau, O. Onar, and D. M. Ionel, "Three and two phase rotating field inductive couplers for wireless power transfer with one phase per layer winding," in *2025 IEEE Transportation Electrification Conference & Expo (ITEC)*, 2025.

[14] R. Zeng, O. C. Onar, M. Mohammad, G. Su, E. Asa, and V. P. Galigekere, "Modeling and analysis of a polyphase wireless power transfer system for ev charging applications," in *2022 IEEE Applied Power Electronics Conference and Exposition (APEC)*, 2022, pp. 1885–1890.

[15] X. Yu, J. Feng, L. Zhu, and Q. Li, "Coil optimization of a planar omnidirectional wpt system," in *2024 IEEE Energy Conversion Congress and Exposition (ECCE)*, 2024, pp. 2054–2060.

[16] M. Rastegar, M. H. Ghaderi, and M. B. Fard, "On balancing of dynamic wireless power transfer system in the presence of misalignment and load variation," in *2024 IEEE Energy Conversion Congress and Exposition (ECCE)*, 2024, pp. 1909–1916.

[17] *Ansys® Electronics, Maxwell, version 25.1, 2025, ANSYS Inc.*

[18] S. Paul, M. Abdelraziq, U. Pratik, and Z. Pantic, "Development of an autonomous wireless charging system for unmanned aerial vehicles," in *2023 IEEE Energy Conversion Congress and Exposition (ECCE)*, 2023, pp. 2127–2133.

[19] T. Jarin, P. V. Nisha, B. Deepanraj, and H. Mewada, "Comparison of PCB and conventional power transfer coils in magnetic coupler designs for electric vehicles," in *2024 International Conference on Smart Systems for applications in Electrical Sciences (ICSSES)*, 2024, pp. 1–6.

[20] F. Marcolini, G. D. Donato, F. Giulii Capponi, M. Incurvati, and F. Caricchi, "On winding manufacturing technologies for coreless axial-flux permanent-magnet machines," in *2023 IEEE Workshop on Electrical Machines Design, Control and Diagnosis (WEMDCD)*, 2023, pp. 1–7.

[21] A. Ramezani and M. Narimani, "An efficient PCB based magnetic coupler design for electric vehicle wireless charging," *IEEE Open Journal of Vehicular Technology*, vol. 2, pp. 389–402, 2021.

[22] "Litz Wire, 14 AWG Unserved Single Build, 5X52/38 Stranding, Ideal for 100 kHz Applications - 6 Spool Sizes." [Online]. Available: https://www.remingtonindustries.com/magnet-wire/litz-wire-14-awg-unserved-single-build-5x52-38-stranding-ideal-for-100-khz-applications-6-spool-sizes/

[23] L. A. Gastineau, D. D. Lewis, and D. M. Ionel, "Combined 3D FEA and machine learning design of inductive polyphase coils for wireless EV charging," in *2024 13th International Conference on Renewable Energy Research and Applications (ICRERA)*, 2024, pp. 1811–1816.

[24] Y. Wu, D. Zhao, Y. Jiang, Y. Li, X. Yu, S. Wang, M. Wu, X. Wang, and Y. Tang, "Precise coil inductance prediction with transfer learning improved deep neural networks in WPT systems," in *2024 IEEE Energy Conversion Congress and Exposition (ECCE)*, 2024, pp. 2092–2098.